HHS Public Access

Author manuscript

Acta Biomater. Author manuscript; available in PMC 2022 March 01.

Published in final edited form as:

Acta Biomater. 2021 March 01; 122: 101–110. doi:10.1016/j.actbio.2020.12.042.

4D Printing of Shape-memory Polymeric Scaffolds for Adaptive Biomedical Implantation

Cheng Zhang[a,†], **Dunpeng Cai**[b,†], **Ping Liao**[a], **Jheng-Wun Su**[a], **Heng Deng**[a], **Bongkosh Vardhanabhuti**[c], **Bret D. Ulery**[d], **Shi-You Chen**[b,*], **Jian Lin**[a,*]

[a]Department of Mechanical and Aerospace Engineering, University of Missouri, Columbia, Missouri 65211, United States

[b]Department of Surgery, University of Missouri, Columbia, Missouri 65211, United States

[c]Food Science Program, Division of Food Systems & Bioengineering, University of Missouri, Columbia, Missouri 65211, United States

[d]Department of Biomedical, Biological & Chemical Engineering, University of Missouri, Columbia, Missouri 65211, United States

Abstract

4D printing has shown great potential in a variety of biomedical applications due to the adaptability and minimal invasiveness of fabricated devices. However, commonly employed shape memory polymers (SMPs) possess undesirable transition temperatures (T_{trans}s), leading to complications in implantation operations. Herein, we demonstrate 4D printing of a new SMP named poly(glycerol dodecanoate) acrylate (PGDA) with a T_{trans} in a range of 20 °C - 37 °C making it appropriate for shape programming at room temperature and then shape deployment within the human body. In addition, the material possesses suitable rheological properties to allow for the fabrication of a variety of delicate 3D structures such as “triangular star”, “six-petal flower”, “honeycomb”, “tube”, tilted “truncated hollow cones”, as well as overhanging “bridge”, “cage”, and “mesh”. The printed 3D structures show shape memory properties including a large fixity ratio of 100% at 20 °C, a large recovery ratio of 98% at 37 °C, a stable cyclability of > 100 times, and a fast recovery speed of 0.4 s at 37 °C. Moreover, the Young’s moduli of the printed structures can be decreased by 5 times due to the phase transition of PGDA, which is compatible with biological tissues. Finally, *in vitro* stenting and *in vivo* vascular grafting demonstrated the geometrical and mechanical adaptivity of the printed constructs for biomedical implantation. This newly developed PGDA SMP based 4D printing technology has the potential to pave a new route to the fabrication of shape memory scaffolds for personalized biomedical applications.

* LinJian@missouri.edu (J. L.), scqvd@missouri.edu (S. Y. C.).

†These authors contribute equally to this work

Declaration of interests

☒ The authors declare that they have no known competing financial interests or personal relationships that could have appeared to influence the work reported in this paper.

Graphical Abstract

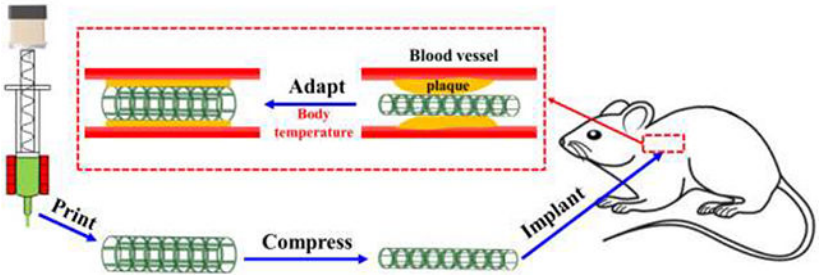

Keywords

4D printing; shape memory polymers; body temperature; biomedical scaffold

1. Introduction

Implantable scaffolds based on heat-responsive shape memory polymers (SMPs)[1] have demonstrated unique properties desirable for biomedical applications[2–4]. In general, a shape memory scaffold (SMS) is first fabricated in a permanent shape designed to fit a geometry of a target physiological environment. Then, the SMS is heated above its transition temperature (T_{trans}), which is equal to either the melting temperature (T_m) for a semi-crystalline polymer or the glass transition temperature (T_g) for an amorphous polymer, for shape programming[5]. At this elevated temperature, the scaffold is deformed to a temporary shape amenable to implantation. Subsequently, this temporary shape is fixed by cooling down to a temperature below T_{trans}. After implantation, the SMS is heated above T_{trans} triggering recovery to the permanent shape that adapts to the target physiological geometry. Often this approach is leveraged to minimize invasiveness during SMS implantation[6–11]. However, such adaptive capability is often compromised when traditional fabrication methods such as molding[3, 6, 8–11], spin-coating[7], or electrospinning[12] are used to fabricate a SMS. While these approaches usually can facilitate the generation of two-dimensional (2D) structures[3, 9, 11], or limited three-dimensional (3D) structures such as curve[7, 8, 12] and twining[6, 10], they cannot well match the intricacies of complex 3D structures like tissues and organs.

Emergence of additive manufacturing, or 3D printing, has fortunately provided a new way to fabricating SMSs with complex geometries[13], As the employed SMPs are active materials that evolve their shapes, properties, or functions over time, this new approach is termed “4D printing”, where time is the fourth dimension[5, 14–17]. Since its inception[18], 4D printing has been applied to fabricate SMSs, such as cell scaffolds[19, 20], vascular stents[21–23], bone implants[24, 25], tracheal scaffolds[26, 27], and atrial septal defect occluder[28]. However, T_{trans} of the SMSs made by 4D printing to date are not desirable for biomedical applications as they are either lower than the room temperature (≤ 20 °C)[19, 20] or higher than the body temperature (> 37 °C)[21–28], as shown in Table S1. This limitation makes fixation of the temporary shape or recovery of the permanent shape under the appropriate conditions a grand challenge. Therefore, 4D printing of a biocompatible SMP with T_{trans} in

the range of 20 °C to 37 °C and suitable printability is necessary for the biomedical implantation applications.

To tackle this challenge, we report the 4D printing of a new SMP, *i.e.*, poly(glycerol dodecanoate) acrylate (PGDA), which is synthesized via modification of our previously developed biodegradable SMP poly(glycerol dodecanoate) (PGD)[29, 30]. Our previous work showed the T_{trans} of PGD can be tuned to the range of 22.5 °C to 43.6 °C by altering synthesis conditions[29]. Despite this work, employment of thermoset PGD as a material for 4D printing has not yet been demonstrated due to common problems inherent to thermoset polymers: lack of printability, easy collapse of printed structures, and high temperature curing requirement[31]. To solve these problems, we modified PGD into a photo-curable PGD, named PGDA through the incorporation of acrylate groups. Benefitting from its suitable rheological properties, a variety of 3D structures were printed. These structures show a large fixity ratio of 100% when programmed at 20 °C, a recovery ratio of 98% at 37 °C, a cycling stability of greater than 100 times, and short recovery time of 0.4 s at 37 °C. The Young's moduli of the structures become more comparable to that of soft biological tissues at 37 °C, thus reducing the mechanical mismatch between the printed scaffolds and biological tissues after implantation. To demonstrate potential applications in biomedical implantation, the printed structures for vascular stents and vascular grafts were tested *in vitro* and *in vivo*, respectively.

2. Materials and Methods

2.1 Polymer synthesis and modification

PGD prepolymer (Pre-PGD) was synthesized according to our previously published approach[29]. Glycerol (99%, synthetic, ACROS Organics) and dodecanedioic acid (DDA, 99%, Alfa Aesar) were mixed in a three-necked flask at a molar ratio of 1:1. The mixture was heated to 120 °C in an oil bath under nitrogen flow and magnetic stirring for 24 h. To synthesize PGDA, Pre-PGD was modified via an acrylation reaction. In detail, 20 g of Pre-PGD was first dissolved in a base solution, which was prepared by mixing 0.1 g of 4-methoxyphenol (99%, Acros Organics), 0.2 g of 4-(dimethylamino) pyridine (99%, Alfa Aesar), 3.56 mL of triethylamine (Fisher Chemical), and 200 mL of methylene dichloride (Fisher Chemical). The Pre-PGD solution was cooled to 0 °C under nitrogen flow for 10 min after which 3 mL of acryloyl chloride (96%, Alfa Aesar), pre-diluted in 30 mL methylene dichloride, was slowly added. The reaction vessel was then sealed with aluminum foil and stirred at room temperature. After reacting overnight (~ 12 h), an additional 0.1 g of 4-methoxyphenol was added. The solution was dried by removing the methylene dichloride in a rotary evaporator and subsequently dissolved in 100 mL of ethyl acetate (99%, Acros Organics). The solution was centrifuged at 10,000 rpm for 10 min to isolate the solid triethylamine salt by-product from the solubilized PGDA. The supernate was dried in the rotary evaporator and dissolved again in methylene dichloride containing 0.1 g of the photo initiator 2,2-dimethoxy-2-phenylacetophenone. Finally, the solution was dried to obtain a printable PGDA powder.

2.2 Printing process

An extrusion head (TAM-15, Hyrel 3D) with a built-in heater was mounted to the printer (Engine SR, Hyrel 3D). A nozzle (TLHOME) with an inner diameter of 600 μm (M20) was attached to the end of the extrusion head and wrapped by an additional heater to avoid clogging of the nozzle caused by possible PGDA solidification during ink flow. PGDA was loaded into the container of the extrusion head and heated to 45 °C by the built-in heater. Various 3D structures were designed by CAD software (SolidWorks) and converted to G-code scripts using a slicing software (Slic3r) to control the printer and the extrusion head. The printed structures were irradiated for 10 min by UV light with an intensity of 10 mW cm^{-2} followed by thermal curing in an oven at 145 °C for various durations.

2.3 Materials Characterization

Flow behavior of PGDA was measured by a Kinexus Pro rheometer (NETZSCH Instruments North America, LLC, Burlington, MA) with a plate-plate geometry (diameter of 50 mm) and 1 mm gap. A Thermo Nicolet 380 FTIR Spectrometer with DIAMOND ATR was used to collect FTIR spectra. DSC measurements were taken with a TA Q10where the temperature was held at 0 °C for 1 min followed by ramping from 0 to 70 °C at a constant rate of 20 °C min^{-1}. A motorized test stand (Mark-10 ESM303) was utilized to conduct tensile tests following standard methods outlined in ASTM D638.

2.4 Anastomosis of printed tube to mouse aorta

A mouse model of aortic transplantation was performed following well-established method[32]. Briefly, recipient mice were anesthetized with a mixture of 1.5% (by volume) isoflurane and 100% oxygen through a face mask followed by hair removal and disinfection of the skin in the abdominal area. A mid-line incision from the xiphoid to the pelvis was made. The infrarenal aorta between renal arteries was dissected and small branches of this segment were secured using 11–0 monofilament suture. Proximal and distal portions of the aorta were clamped and the tissue between the clamps was cut and flushed with saline. The printed tube was placed in the orthotopic position and anastomosed to the recipient's proximal and distal ends of the abdominal aorta with an end-to-end pattern using 11–0 polyamide monofilament suture. Clamps on both sides were then carefully removed and visible pulses on the graft were observed. The abdominal contents were returned to the abdominal cavity and the wound was closed with 4–0 polyglycolic acid suture. Animals were euthanized 7 or 14 days after transplantation. The printed tube, along with the tissues attached to the tube, were removed and fixed with 4% Paraformaldehyde (PFA), embedded in 2% paraffin, sectioned on a microtome, and then analyzed using different histological stains. The animal surgery procedure was approved by the Institutional Animal Care and Use Committee of University of Missouri.

2.5 Histology

The paraffin sections of the printed tube were subjected to Hematoxylin and Eosin (H & E), Elastica van Gieson (EVG), and Picro Sirius Red (PSR) staining using standard procedures and reagents from StatLab (McKinney, TX, USA) following manufacturers' recommendations. Stained images were captured using a Nikon microscope.

2.6 Immunofluorescence (IF) staining

An immunofluorescence assay was performed as previously described[33]. Fixed sections of transplanted 4D-printed tube had their paraffin removed and were then hydrated. After rinsing with PBS, sections were permeabilized with 0.5% Triton X100 in PBS and blocked with 2% BSA for 1 h at room temperature. Sections were then incubated overnight with VE-Cadherin or a-SMA antibody at 4 °C followed by 1 h of incubation with fluorescent dye-conjugated secondary antibody at room temperature. After three washes with PBS, sections were mounted using antifade reagent containing DAPI. Images were captured using a Nikon Fluorescent microscope.

2.7 Statistical analysis

Each type of experiments was repeated at least three times. Statistical analysis was performed using single-factor analysis of variance (ANOVA) and values were presented as mean ± standard deviation. $P < 0.05$ was considered to indicate a statistically significant difference.

3. Results and discussion

3.1 Synthesis of PGDA

Thermoset polymers are usually quite difficult to be 3D printed. If they are cured before printing, it is hard to extrude them through a printing nozzle. If they are cured after printing, the printed structure is weak and may easily collapse[31]. As a type of thermoset polymers, the PGD is no exception to this issue[30]. So in order to retain printed structures of uncured PGD, a high-temperature curing process that enables crosslinking is required. As shown in Figure S1, a “six-petal flower” structure was printed from a uncured PGD prepolymer (Pre-PGD, T_m = 43.7 °C[29]). When heated to 120 °C to further crosslink the PGD, the structure melted and collapsed. Whereas, if PGDA, a photocurable derivative PGD, was employed, printed 3D structures can be well retained due to the formation of an internal phonto-crosslinked network.

The fabrication steps of a 3D printed PGDA scaffold are illustrated in Figure 1a with corresponding chemical reactions provided in Figure S2. First, PGD prepolymer (Pre-PGD) was synthesized via polycondensation of glycerol and dodecanedioic acid (DDA) (Figure 1a–i). In Pre-PGD, linear polyester chains with little crosslinked polyester network formation dominate Thus, the printed structures easily collapse upon heating (Figure S1). Then, the Pre-PGD was functionalized to have photo-curability via an acrylation reaction[34] by introducing acryloyl groups to the PGD’s polyester chains (Figure 1a–ii). The resulting poly (glycerol dodecanoate) acrylate (PGDA) can be photocurable under UV light to form Photo-crosslinked PGDA (PHc-PGDA). To confirm Pre-PGD acrylation and PGDA photo-crosslinkability, Fourier transform infrared (FTIR) spectra of Pre-PGD, PGDA, and Photo-crosslinked PGDA (PHc-PGDA) were collected (Figure S3). The peaks at 2850−2950 cm^{-1}, 1690−1780 cm^{-1}, and 1020−1250 cm^{-1} represent C-H, C=O, and C-O bonds[35], respectively, all common bonds in these polymers. The characteristic peak of vinyl C=C at 1639 cm^{-1} only appears in the PGDA spectrum, suggesting that vinyl C=C bonds are successfully introduced to the Pre-PGD polyester chains by the acrylation reaction

and then consumed during PGDA photo-crosslinking. PGDA was separated by centrifugation and dissolved in methylene chloride where photo initiator was introduced. After drying, the PGDA was ready for printing.

3.2 Printing and curing of the shape memory polymer

The printing was performed using a commercial 3D printer (Figure S4a) employing an extrusion head that can be heated (Figure S4b). PGDA powder was first loaded into the container of the extrusion head and then heated into a viscous state to facilitate polymer flow through the nozzle. A representative 3D structure, a "triangular star", was designed and converted to G-code, which was used to control the printer stage as the printing head extruded PGDA (Figure 1a–iii). After the extruded PGDA was cooled down to room temperature naturally, it was irradiated by UV light with a wavelength of 365 nm and intensity of 10 mW cm^{-2}. The irradiation time was set to 10 min which should be sufficient for the photo-polymerization reactions of the acrylated polyesters[34, 36]. PHc-PGDA (Figure 1a–iv) can retain its printed structure even when thermally cured at a temperature of 145 °C for 6 hours in an oven to yield thermally crosslinked PGDA (Tc-PGDA, Figure 1a–v). The fabricated "triangular star" structure displayed shape memory behavior (Figure 1b and Movie S1). It was initially deformed to a temporary shape, such as a compressive "clover", when heated above T_{trans}, and then fixed by cooling down below T_{trans}. Once the structure was heated above T_{trans}, the "clover" shape recovered to its original "triangular star" shape within eight seconds.

3.3 Thermal and rheological properties of PGDA

To help optimize the printing process, the thermal and rheological properties of PGDA were investigated. Differential scanning calorimetry (DSC) was performed to study the thermal property of the PGDA with a DSC curve plotted in Figure 2a. Two endothermic peaks at 25 °C and 45 °C were observed, indicating the semi-crystalline nature of PGDA. In PGDA, partial DDA molecules are crosslinked to form amorphous polyester network while the remaining DDA molecules are grafted rather than crosslinked to form crystalline domains[29]. During heating, re-perfection and variation of the crystalline domains result in the first peak at a lower temperature, while melting results in the second peak at a higher temperature[37]. The second peak at 45 °C is defined as the melting temperature (T_m), which is also the T_{trans} for PGDA and was chosen as the printing temperature. We further studied the rheological properties of PGDA using a rheometer. Viscosity as a function of the shear rate of a PGDA sample was measured at 25 °C (Figure 2b). The viscosity exponentially decreased with increased shear rates from 323.9 Pa-s (at a shear rate of 1 s^{-1}) to 10.2 Pa-s (at a shear rate of 200 s^{-1}), a phenomenon known as shear-thinning[38]. Usually, a shear-thinning material is suitable for extrusion-based printing because it will flow under the high shear conveyed by the motor while rapidly retaining its printed structure post-deposition when it is under low shear. However, the following calculation indicates that the shear rate used in printing is too low to create such a shear-thinning effect for successfully extruding PGDA out at a temperature of 25 °C or less. The shear rate (γ) at the inner wall of a nozzle is defined as[39]

$$\gamma = 4Q/\left(\pi r^3\right) \quad (1)$$

where r is the radius of the nozzle and Q is the flow rate, calculated by

$$Q = mWHS \quad (2)$$

where m is the flow rate multiplier, W is the extrusion width, H is the extrusion height, and S is the printing speed. By substituting the printing parameters used into these equations, γ is calculated to be ~ 10 s^{-1} (Table S2). As shown in Figure 2b, the corresponding viscosity at 25 °C is 72.4 Pa-s, which is much larger than value (< 20 Pa-s) that can ensure printing materials while readily flow through the nozzle[22, 40]. This result suggests that the PGDA cannot be printed out by a simple shear-thinning effect at 25 °C or less.

Fortunately, the thermo-rheological properties of PGDA suggests that increasing temperature will enhance its printability. We measured the flow behavior of PGDA at temperatures ranging from 20 °C to 80 °C. At 20 °C, the viscosity exceeded the upper limit of the rheometer whereas the relationship between viscosity and the shear rate was measurable from 30 °C - 80 °C using 5 °C intervals (Figure 2c). The viscosity of PGDA in this temperature range does not change much as the shear rate increases, indicating an elimination of a shear-thinning effect. However, as expected, viscosity does decrease as temperature increased. For example, the viscosity at a shear rate of 10 s^{-1} significantly decreases from 72.4 Pa-s to 2.4 Pa-s when the printing temperature is increased from 25 °C to 30 °C, and further decreases to 0.13 Pa-s when the temperature is increased to 80 °C (Figure 2d). This data suggests that PGDA can smoothly flow through the nozzle at a temperature of 30 °C or more, and then retain a printed shape after being cooled to 25 °C or lower due to a rapid rise in viscosity. Therefore, in our work, printing and substrate temperatures were set at 45 °C and 20 °C, respectively (Figure S4c).

3.4 Shape memory properties

After a PGDA structure was printed, UV light was first used to crosslink the polymer followed by thermally curing it for various durations. Herein, PHc-PGDA (photo-crosslinked but not thermally cured) and Tc-PGDA (photo-crosslinked and thermally cured) samples are collectively abbreviated as c-PGDA. We first systematically studied how the T_{trans} of c-PGDA is affected by photo-crosslinking and thermal curing using DSC. DSC curves of c-PGDA samples which were thermally cured for various durations were shown in Figure 3a. The PHc-PGDA exhibits the two close endothermic peaks to those of PGDA. As thermal curing duration increases, the lower endothermic peak gradually disappears, indicating the more crystalline domains of the polymer become amorphous. Because more DDA molecules in the crystalline domains are crosslinked to form an amorphous network[29]. Figure 3b shows T_{trans} identified from the DSC curves of the c-PGDA samples prepared with thermal curing durations of 0, 2, 4, 6, and 8 h. It shows that T_{trans} decreases from 46.6 °C to 21.5 °C as thermal curing duration increases to 8 h. As T_{trans} is known to correlate with the ratio of the crystalline domains[41], the observed results correspond with the established understanding.

Shape memory properties of printed c-PGDA structures were then systematically investigated. The shape fixity and recovery of various c-PGDA products were characterized by a thermomechanical bending test[42]. As shown in Figure S6, a c-PGDA strip was first heated to 37 °C in a water bath and then deformed to a set deformation angle (θ_d). The bent shape is then fixed by cooling the specimen in 20 °C water under external stress. After removal of the stress, the bent specimen recovers its shape to a fixed angle (θ_f). Once the specimen is heated again to 37 °C, it is expected to shift to a recovery angle (θ_r). The shape fixity ratio (R_f) and shape recovery ratio (R_r) are calculated by

$$R_f = (\theta_f/\theta_d) \times 100\% \quad (3)$$

$$R_r = (\theta_f - \theta_r)/\theta_f \times 100\% \quad (4)$$

R_f and R_r of c-PGDA with varying thermal curing duration are plotted in Figure 3c–d, respectively. R_f of the samples which were c-PGDA thermally cured for 0 – 6 hours are close to 100%, while c-PGDA with 8 hours of thermal curing has a R_f of 80%. The decreased R_f is beccause the cooling temperature (20 °C) is too close to the T_{trans} (21.5 °C) resulting in incomplete phase transition. Similarly, R_r of the c-PGDA samples which were thermally cured for 4–8 hours was found to be > 98% since their T_{trans} are lower than 37 °C, the deployment temperature used in this study. Moreover, the cyclability and the recovery rate of the c-PGDA were studied. A sample thermally cured for 6 hours maintains a R_f of ~100% and a R_r of ~98% after 100 cycles (Figure 3e). It is able to recover to its permanent shape in just 1.4 s when heated to 25 °C. This recovery time decreases as the stimulation temperature increases, going down to ~ 0.4 s at 37 °C (Figure 3f, Movie S2). This highly desirable shape memory performance is influenced by the semi-crystalline nature of c-PGDA (Figure S5). The covalent, amorphous PGDA regions maintain the permanent shape. Once heated, the crystal DDA is melted and the sample can be deformed by an external stress. The deformed shape is fixable at a lower temperature due to the re-crystallization of the DDA regions. Once the sample is heated above T_{trans}, the DDA region melts again allowing the PGDA network to recover to its permanent shape.

3.5 Mechanical properties

The mechanical properties of c-PGDA were also evaluated by tensile testing, from which the extent of crosslinking can be estimated. The stress-strain curves taken below and above T_{trans} of a c-PGDA sample were plotted in Figure 4a. At 20 °C (below T_{trans}), the c-PGDA shows elastic deformation until a strain of < 15%. The calculated Young's modulus is 15.4 MPa. Beyond the strain of 15%, the deformation becomes plastic and it fractures at an ultimate stress of 5.1 MPa at strain of 210%. Interestingly, at 37 °C (above T_{trans}), the c-PGDA shows elastic deformation with a fracture strength of 1.1 MPa at a strain of 35.5%. This indicates that the polymer network possesses rubber characteristics after the phase transition[43]. The calculated Young's modulus of 3.2 MPa is comparable to some soft biological tissues such as blood vessels whose modulus is in the range of 0.6 to 3.5 MPa[44] making it suitable for certain biomedical applications. This mechanical adaptability may promote the tissue growth, which will be discussed later. The crosslinking density of c-

PGDA can be also derived from the Young's modulus at the rubbery state based on the theory of rubber elasticity[45]:

$$n = E\,(3RT)^{-1} \tag{5}$$

where n is the crosslinking density (mol m^{-3}), E is the rubbery state Young's modulus (Pa), R is the ideal gas constant (8.314 J mol^{-1} K^{-1}), and T is absolute temperature (K). Using the data generated, the estimated crosslinking density of c-PGDA was found to be 393.6 mol·m^{-3}. Stress-strain curves of the samples with thermal curing durations of 0, 2, 4, and 8 h were also measured at temperatures above T_{trans} (Figure S6). Their Young's moduli and crosslinking densities were calculated and plotted in Figure 4b. Without thermal curing, c-PGDA has a very low modulus (0.235 MPa) and crosslinking density (28.7 mol m^{-3}). This relatively low crosslinking degree is also indicated in the material's FTIR spectrum (Figure S3), which shows very low intensity of vinyl C=C peaks. As thermal curing duration increases, the modulus and crosslinking density also increase. At 8 h, they reach 3.315 MPa and 405.0 mol·m^{-3}, respectively, which are more than 14 times of those for the sample without thermal curing.

3.6 3D structures

The aforementioned systematic material characterizations indicated that PGDA can be used to print various 3D structures. The first group of 3D architectures was realized by vertically stacking multiple layers (Figure 5a), including a "six-petal flower", a "honeycomb", and a "tube". It is worth mentioning that the "tube" structure did not collapse even with a large aspect ratio (L/D = 10). Its geometry is similar to that of medium-sized human arteries (inner diameter = 4 mm, wall thickness = 1 mm)[46], which would make it useful as a vascular graft. In addition, tilted 3D structures can be readily printed (Figure 5b). According to the "45 degree rule", it is challenging for extrusion-based 3D printing to be used to fabricate a structure with a tilting angle > 45°[47]. With PGDA, we have been able to print "truncated hollow cone" structures with tilting angles of 30°, 45°, and 60°. Moreover, overhanging 3D structures (tilting angle equals 90°) were achieved (Figure 5c), including a "bridge", a "cage", and a "mesh". The successful printing of these tilted and overhanging 3D structures can be mainly attributed to the improved printability of PGDA.

3.7 Geometrically adaptive vascular stent

For functional demonstration of the geometrical adaptation of the printed scaffolds for potential biomedical implantation, an *in vitro* test of a printed vascular stent was performed. A mesh stent was first printed from PGDA, then photo-crosslinked and thermally cured for 6 hours. After that, it was programmed by twisting and wrapping on a glass tube (5 mm diameter) to a temporary and compact shape above T_{trans} for easy delivery (Figure 6a–b). After that, it was implanted to a purposely compressed region in the middle of a silicone tube simulating a narrowed blood vessel (Figure 6c). After heating above T_{trans}, the stent deployed recovering its permanent shape by releasing its stored energy. As it is constrained by the wall of the silicone tube, the residual stress in the stent during the shape recovery imposes force on the wall of the silicone tube, enlarging the tube diameter from 4.5 mm to

7.5 mm (Figure 6d). This process mimics stenting surgery where imposed force to the vascular wall would help to prevent re-narrowing of the blood vessel.

3.8 Mechanically adaptive vascular graft

Another function of printed c-PGDA is as a mechanically adaptive and biocompatible scaffold in the treatment of vascular disease. First, a tube structure was first printed from PGDA, which was then photo-crosslinked and post-cured for 6 hours (Figure 5a). Then it was implanted into a mouse aorta as a vascular graft (Figure 7a). We first opened the surgery area, ligatured the two ends of the targeted blood vessel, and then drained the inside blood. As the temperature of the surgery area was lower than the body temperature, it took a longer time for the shape deployment than that operated under a temperature-controlled environment. Thus, the vascular graft did not recover until the implantation procedure was finished and the blood started to flow though the graft. After 14 days, tissue had adhered to the inner and outer surface of the printed tube (Figure 7b) which was further analyzed by H&E and EVG staining (Figure 7c–f). The outer surface appeared to be populated with adipocytes and connective tissue or adventitial cells (Figure 7c–d). More interestingly, elastin fibers, although without typical mature elastin lamina structure, were observed to be lining the inner and outer surface of the tube (Figure 7e–f). Immunostaining showed that endothelial cells, as shown by VE-Cadherin staining, were lining the inner surface of the tube (Figure 7g) while a-SMA-positive cells were present on the outer surface (Figure 7h), suggesting the presence of adventitial fibroblasts or medial smooth muscle cells. VE cadherin-expressing cells lining the inner surface is significant because it suggests that the printed c-PGDA graft provides a biocompatible environment, especially appropriate modulus, for the attachment and growth of endothelial cells that would eventually form the endothelium for a blood vessel. The presence of the endothelial layer is essential for maintaining the vessel barrier, preventing coagulation, and controlling blood flow. In addition, the presence of α-SMA-positive cells and adipocytes in the outer surface suggests that tentative medial and adventitial layers are being formed around the graft. Since fabrication of biocompatible and degradable constructs that replicate the complexity and functionality of native arteries or veins remains a significant challenge, our results demonstrate the exciting potential of synthetic c-PGDA materials for arterial grafting applications.

4. Conclusions

In summary, we have demonstrated the 4D printing potential of a new SMP, PGDA, whose T_{trans} is appropriate for shape programming at room temperature and shape deployment at body temperature. Its suitable thermo-rheological properties enable the printing of multifunctional 3D structures, not only including commonly stacked structures, but tilted and overhanging structures as well which have previously proven challenging for other printing materials to achieve. We introduced a photo-crosslinking strategy to overcome common issues associated with printing thermoset polymers. The printed constructs showed great shape memory properties including high shape fixity and recovery ratios, cycling stability, and fast recovery time. The geometrical and mechanical adaptivity of the printed scaffolds have been demonstrated in an *in vitro* stenting test and an *in vivo* grafting

procedure. Potential formation of a well-structured blood vessel when used for vascular grafting shows its promise for clinical applications such as arterial grafting.

Supplementary Material

Refer to Web version on PubMed Central for supplementary material.

Acknowledgment

This work was financially supported by grants from the National Science Foundation (award number: 1825352), the United States Department of Agriculture (award number: 2020-67030-31336), and the National Institutes of Health (1R03EB028922-01, HL119053, and HL147313).

References

[1]. Lendlein A, Kelch S, Shape-memory polymers, Angew. Chem. Int. Ed 41(12) (2002) 2034–2057.

[2]. Lendlein A, Langer R, Biodegradable, Elastic Shape-Memory Polymers for Potential Biomedical Applications, Science 296(5573) (2002) 1673. [PubMed: 11976407]

[3]. Xie R, Hu J, Hoffmann O, Zhang Y, Ng F, Qin T, Guo X, Self-fitting shape memory polymer foam inducing bone regeneration: A rabbit femoral defect study, BBA-Gen. Subjects 1862(4) (2018) 936–945.

[4]. Kirillova A, Ionov L, Shape-changing polymers for biomedical applications, J. Mater. Chem. B 7(10) (2019) 1597–1624. [PubMed: 32254904]

[5]. Kuang X, Roach DJ, Wu J, Hamel CM, Ding Z, Wang T, Dunn ML, Qi HJ, Advances in 4D Printing: Materials and Applications, Adv. Funct. Mater 29(2) (2019) 1805290.

[6]. Ware T, Simon D, Hearon K, Liu C, Shah S, Reeder J, Khodaparast N, Kilgard MP, Maitland DJ, Rennaker RL, Three-Dimensional Flexible Electronics Enabled by Shape Memory Polymer Substrates for Responsive Neural Interfaces, Macromol. Mater. Eng 297(12) (2012) 1193–1202. [PubMed: 25530708]

[7]. Reeder J, Kaltenbrunner M, Ware T, Arreaga-Salas D, Avendano-Bolivar A, Yokota T, Inoue Y, Sekino M, Voit W, Sekitani T, Mechanically adaptive organic transistors for implantable electronics, Adv. Mater 26(29) (2014) 4967–4973. [PubMed: 24733490]

[8]. Montgomery M, Ahadian S, Davenport Huyer L, Lo Rito M, Civitarese RA, Vanderlaan RD, Wu J, Reis LA, Momen A, Akbari S, Pahnke A, Li R-K, Caldarone CA, Radisic M, Flexible shape-memory scaffold for minimally invasive delivery of functional tissues, Nat. Mater 16(10) (2017) 1038–1046. [PubMed: 28805824]

[9]. Yu J, Xia H, Ni Q-Q, A three-dimensional porous hydroxyapatite nanocomposite scaffold with shape memory effect for bone tissue engineering, J. Mater. Sci 53(7) (2018) 4734–4744.

[10]. Zhang Y, Zheng N, Cao Y, Wang F, Wang P, Ma Y, Lu B, Hou G, Fang Z, Liang Z, Yue M, Li Y, Chen Y, Fu J, Wu J, Xie T, Feng X, Climbing-inspired twining electrodes using shape memory for peripheral nerve stimulation and recording, Sci. Adv 5(4) (2019) eaaw1066. [PubMed: 31086809]

[11]. Xuan H, Hu H, Geng C, Song J, Shen Y, Lei D, Guan Q, Zhao S, You Z, Biofunctionalized chondrogenic shape-memory ternary scaffolds for efficient cell-free cartilage regeneration, Acta Biomater 105 (2020) 97–110. [PubMed: 31953195]

[12]. Zhao Q, Wang J, Cui H, Chen H, Wang Y, Du X, Programmed shape-morphing scaffolds enabling facile 3D endothelialization, Adv. Funct. Mater 28(29) (2018) 1801027.

[13]. Placone JK, Engler AJ, Recent Advances in Extrusion-Based 3D Printing for Biomedical Applications, Adv. Healthc. Mater 7(8) (2018) 1701161.

[14]. Ge Q, Qi HJ, Dunn ML, Active materials by four-dimension printing, Appl. Phys. Lett 103(13) (2013) 131901.

[15]. Huang L, Jiang R, Wu J, Song J, Bai H, Li B, Zhao Q, Xie T, Ultrafast Digital Printing toward 4D Shape Changing Materials, Adv. Mater 29(7) (2017) 1605390.

[16]. Wu J-J, Huang L-M, Zhao Q, Xie T, 4D Printing: History and Recent Progress, Chinese J. Polym. Sci 36(5) (2018) 563–575.

[17]. Su J-W, Tao X, Deng H, Zhang C, Jiang S, Lin Y, Lin J, 4D printing of a self-morphing polymer driven by a swellable guest medium, Soft Matter 14(5) (2018) 765–772. [PubMed: 29302670]

[18]. Tibbits S, The emergence of “4D printing”, TED conference, 2013.

[19]. Miao S, Zhu W, Castro NJ, Nowicki M, Zhou X, Cui H, Fisher JP, Zhang LG, 4D printing smart biomedical scaffolds with novel soybean oil epoxidized acrylate, Sci. Rep 6(1) (2016) 27226. [PubMed: 27251982]

[20]. Miao S, Cui H, Nowicki M, Lee S.-j., Almeida J, Zhou X, Zhu W, Yao X, Masood F, Plesniak MW, Mohiuddin M, Zhang LG, Photolithographic-stereolithographic-tandem fabrication of 4D smart scaffolds for improved stem cell cardiomyogenic differentiation, Biofabrication 10(3) (2018) 035007. [PubMed: 29651999]

[21]. Wei H, Zhang Q, Yao Y, Liu L, Liu Y, Leng J, Direct-Write Fabrication of 4D Active Shape-Changing Structures Based on a Shape Memory Polymer and Its Nanocomposite, ACS Appl. Mater. Interfaces 9(1) (2017) 876–883. [PubMed: 27997104]

[22]. Kuang X, Chen K, Dunn CK, Wu J, Li VCF, Qi HJ, 3D Printing of Highly Stretchable, Shape-Memory, and Self-Healing Elastomer toward Novel 4D Printing, ACS Appl. Mater. Interfaces 10(8) (2018) 7381–7388. [PubMed: 29400445]

[23]. Lin C, Zhang L, Liu Y, Liu L, Leng J, 4D printing of personalized shape memory polymer vascular stents with negative Poisson’s ratio structure: A preliminary study, Sci. China Technol. Sci (2020).

[24]. Senatov FS, Niaza KV, Zadorozhnyy MY, Maksimkin AV, Kaloshkin SD, Estrin YZ, Mechanical properties and shape memory effect of 3D-printed PLA-based porous scaffolds, J. Mech. Behav. Biomed. Mater 57 (2016) 139–148. [PubMed: 26710259]

[25]. Zhang F, Wang L, Zheng Z, Liu Y, Leng J, Magnetic programming of 4D printed shape memory composite structures, Compos. Part A Appl. Sci. Manuf 125 (2019) 105571.

[26]. Zarek M, Mansour N, Shapira S, Cohn D, 4D Printing of Shape Memory-Based Personalized Endoluminal Medical Devices, Macromol. Rapid Commun 38(2) (2017) 1600628.

[27]. Zhao W, Zhang F, Leng J, Liu Y, Personalized 4D printing of bioinspired tracheal scaffold concept based on magnetic stimulated shape memory composites, Compos. Sci. Technol 184 (2019) 107866.

[28]. Lin C, Lv J, Li Y, Zhang F, Li J, Liu Y, Liu L, Leng J, 4D-Printed Biodegradable and Remotely Controllable Shape Memory Occlusion Devices, Adv. Funct. Mater. 29(51) (2019) 1906569.

[29]. Zhang C, Deng H, Kenderes SM, Su J-W, Whittington AG, Lin J, Chemically Interconnected Thermotropic Polymers for Transparency-Tunable and Impact-Resistant Windows, ACS Appl. Mater. Interfaces 11(5) (2019) 5393–5400. [PubMed: 30644710]

[30]. Migneco F, Huang Y-C, Birla RK, Hollister SJ, Poly(glycerol-dodecanoate), a biodegradable polyester for medical devices and tissue engineering scaffolds, Biomaterials 30(33) (2009) 6479–6484. [PubMed: 19712970]

[31]. Lei D, Yang Y, Liu Z, Chen S, Song B, Shen A, Yang B, Li S, Yuan Z, Qi Q, Sun L, Guo Y, Zuo H, Huang S, Yang Q, Mo X, He C, Zhu B, Jeffries EM, Qing F-L, Ye X, Zhao Q, You Z, A general strategy of 3D printing thermosets for diverse applications, Mater. Horizons 6(2) (2019) 394–404.

[32]. Au - Qin L, Au - Yu L, Au - Min W, Mouse Models for Graft Arteriosclerosis, J. Vis. Exp (75) (2013) e50290.

[33]. Robertson D, Savage K, Reis-Filho JS, Isacke CM, Multiple immunofluorescence labelling of formalin-fixed paraffin-embedded (FFPE) tissue, BMC Cell Biol 9(1) (2008) 13. [PubMed: 18366689]

[34]. Nijst CLE, Bruggeman JP, Karp JM, Ferreira L, Zumbuehl A, Bettinger CJ, Langer R, Synthesis and Characterization of Photocurable Elastomers from Poly(glycerol-co-sebacate), Biomacromolecules 8(10) (2007) 3067–3073. [PubMed: 17725319]

[35]. Socrates G, Infrared and Raman characteristic group frequencies: tables and charts, John Wiley & Sons2004.

[36]. Yeh YC, Highley CB, Ouyang L, Burdick JA, 3D printing of photocurable poly(glycerol sebacate) elastomers, Biofabrication 8(4) (2016) 045004. [PubMed: 27716633]

[37]. Bajpai O, Panja S, Chattopadhyay S, Setua D, Process–structure–property relationships in nanocomposites based on piezoelectric-polymer matrix and magnetic nanoparticles, Manufacturing of Nanocomposites with Engineering Plastics, Elsevier2015, pp. 255–278.

[38]. Su J-W, Gao W, Trinh K, Kenderes SM, Tekin Pulatsu E, Zhang C, Whittington A, Lin M, Lin J, 4D printing of polyurethane paint-based composites, Int. J. Smart Nano Mater (2019) 1–12.

[39]. Markstedt K, Sundberg J, Gatenholm P, 3D bioprinting of cellulose structures from an ionic liquid, 3D Print Addit. Manuf 1(3) (2014) 115–121.

[40]. Colosi C, Shin SR, Manoharan V, Massa S, Costantini M, Barbetta A, Dokmeci MR, Dentini M, Khademhosseini A, Microfluidic bioprinting of heterogeneous 3D tissue constructs using low-viscosity bioink, Adv. Mater 28(4) (2016) 677–684. [PubMed: 26606883]

[41]. Yao X, Dunn SS, Kim P, Duffy M, Alvarenga J, Aizenberg J, Fluorogel Elastomers with Tunable Transparency, Elasticity, Shape-Memory, and Antifouling Properties, Angew. Chem. Int. Ed 53(17) (2014) 4418–4422.

[42]. Lan X, Liu Y, Lv H, Wang X, Leng J, Du S, Fiber Reinforced Shape-Memory Polymer Composite and Its Application in Deployable Hinge in Space, Smart Mater. Struct 18(2) (2009) 024002.

[43]. Solorio LD, Bocks ML, Hollister SJ, Tailoring the physicochemical and shape memory properties of the biodegradable polymer poly(glycerol dodecanoate) via curing conditions, J. Biomed. Mater. Res. A 105(6) (2017) 1618–1623. [PubMed: 27935209]

[44]. McKee CT, Last JA, Russell P, Murphy CJ, Indentation versus tensile measurements of Young's modulus for soft biological tissues, Tissue Eng. Part B Rev 17(3) (2011) 155–164. [PubMed: 21303220]

[45]. Sperling LH, Introduction to physical polymer science, John Wiley & Sons2005.

[46]. Boron WF, Boulpaep EL, Medical physiology E-book, Elsevier Health Sciences2016.

[47]. Aguilera E, Ramos J, Espalin D, Cedillos F, Muse D, Wicker R, MacDonald E, 3D printing of electro mechanical systems, Proceedings of the Solid Freeform Fabrication Symposium, 2013, pp. 950–961.

Statement of Significance

Adaptive biomedical scaffolds are highly desired for minimally invasive implantation. 4D printing of shape-memory polymers is a promising fabrication technology for such scaffolds. However, currently employed shape-memory polymers have inappropriate transition temperatures resulting in not only complication of implantation operation but also risks of causing frostbite or scald to organs or tissues. Here, we demonstrate 4D printing of a new shape-memory polymer with transition temperature in a range of 20–37 °C. The suitable transition temperature enables printed biomedical scaffolds to be conveniently programed at room temperature and then automatically adapt to physiological environment after being implanted into human body. The 4D printed scaffolds would promote the development of adaptive and personalized biomedical devices.

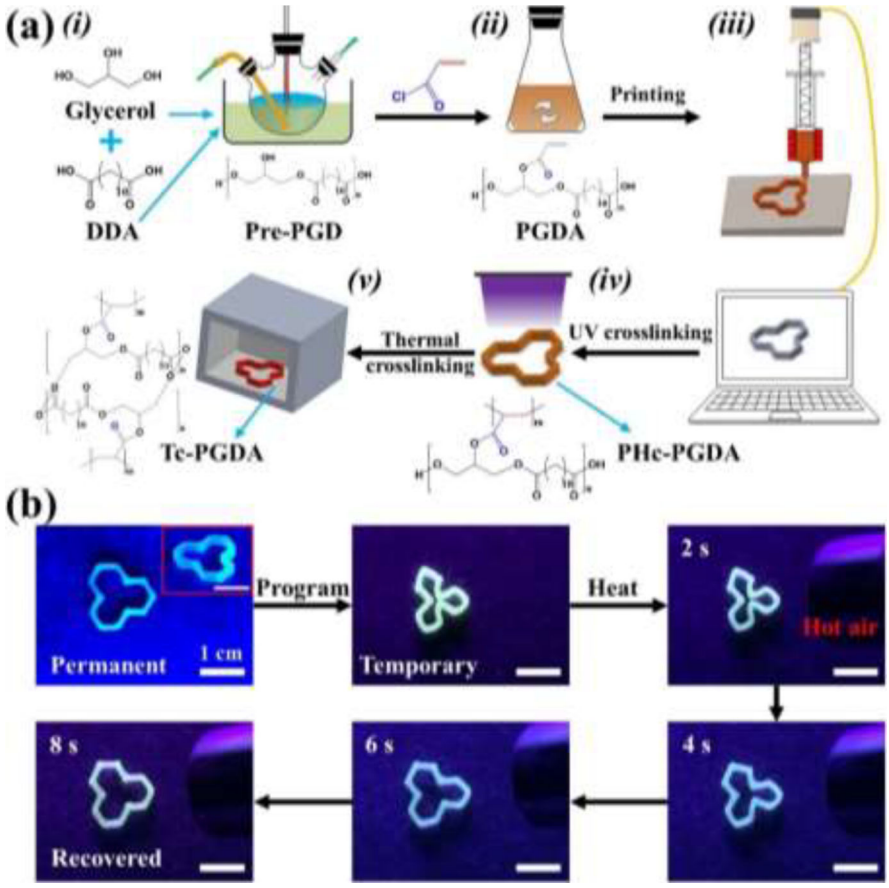

Figure 1.

(a) Schematic of the synthesis and 3D printing process used for PGDA. (b) Photographs showing the shape memory behavior of a printed “triangular star” structure.

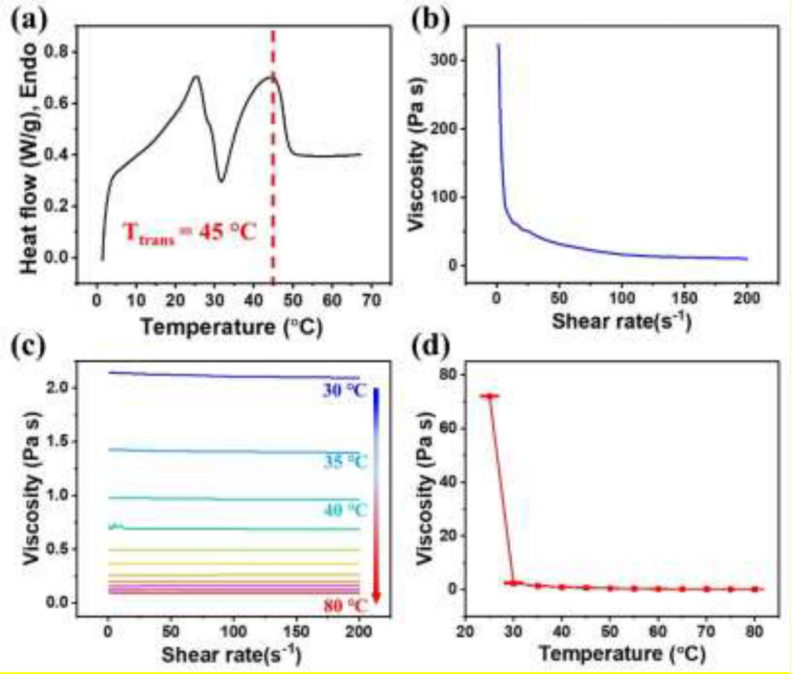

Figure 2.

(a) A DSC curve of a PGDA sample before photo-crosslinking. Viscosity as a function of shear rate was tested at (b) 25 °C and (c) 30 °C - 80 °C. (d) Viscosity as a function of temperature was evaluated at a shear rate of 10 s^{-1}.

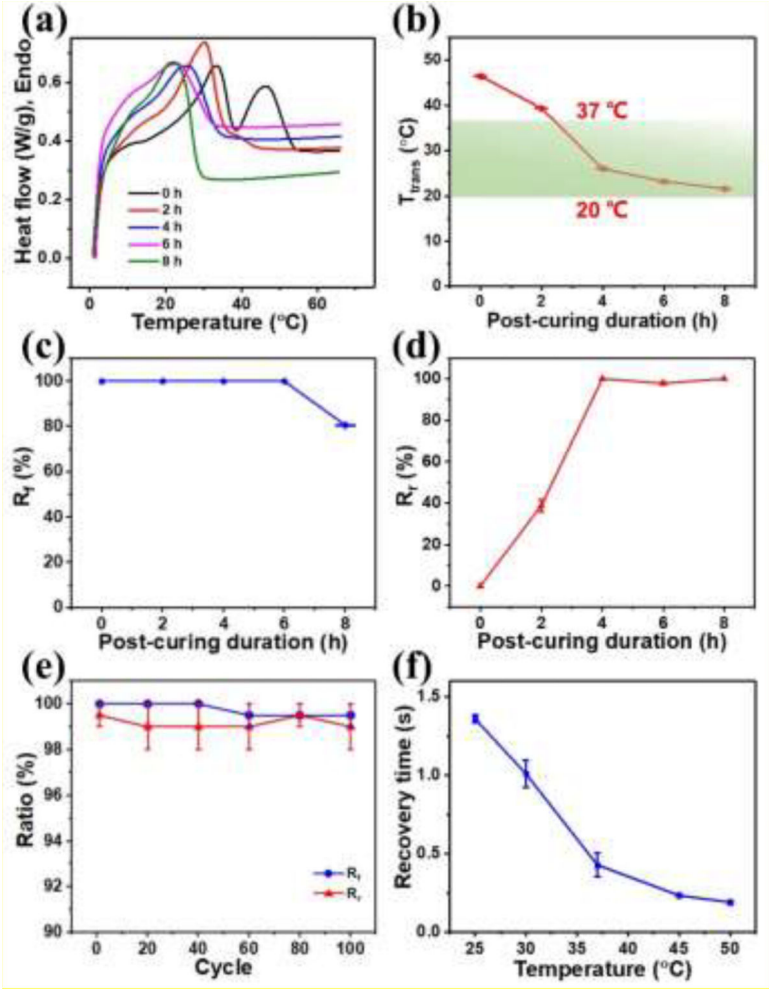

Figure 3.

(a) DSC curves of c-PGDA samples post-cured for 0–8 h. (b) Transition temperature (T_{trans}), (c) shape fixity ratios (R_f, at 20 °C), and (d) shape recovery ratios (R_r, at 37 °C) of c-PGDA samples thermally cured for 0 – 8 h. (e) Cycling performance and (f) recovery time as a function of stimulating temperature of c-PGDA thermally cured for 6 h.

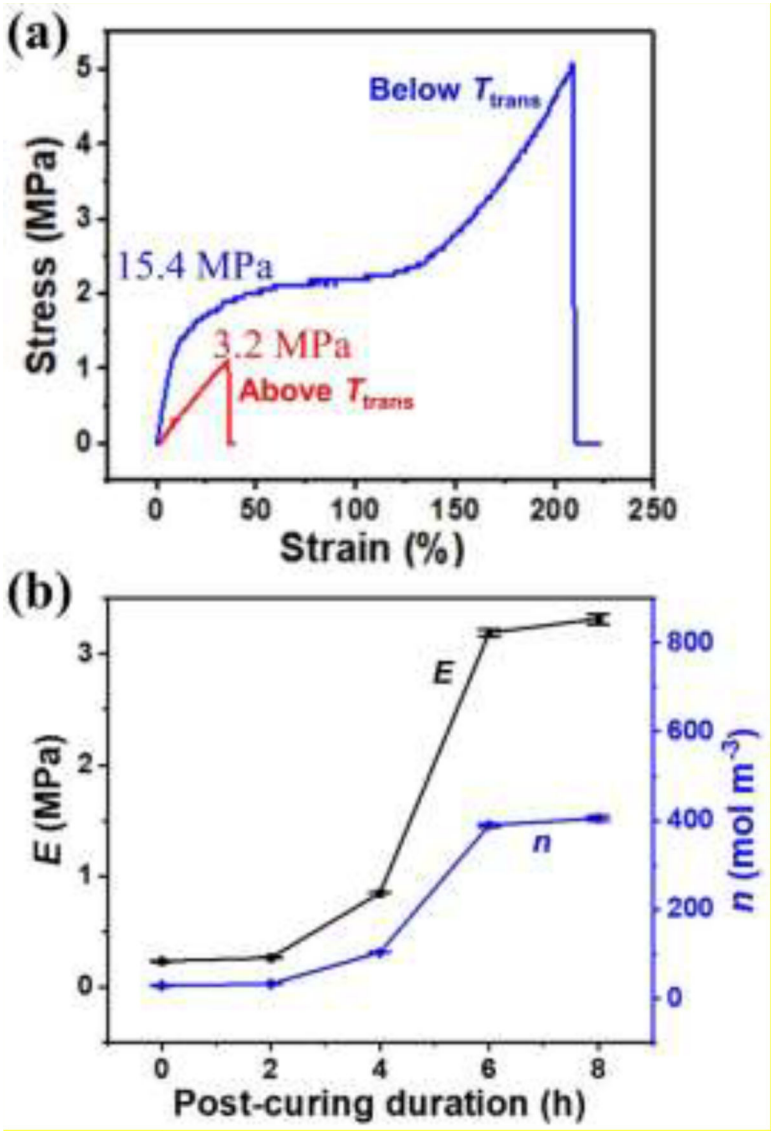

Figure 4.

(a) Representative stress-strain curves of c-PGDA samples thermally cured for 6 h, measured at 20 °C (below T_{trans}) and 37 °C (above T_{trans}). (b) Young's moduli (E) and crosslinking densities (n) of c-PGDA samples thermally cured for 0–8 h.

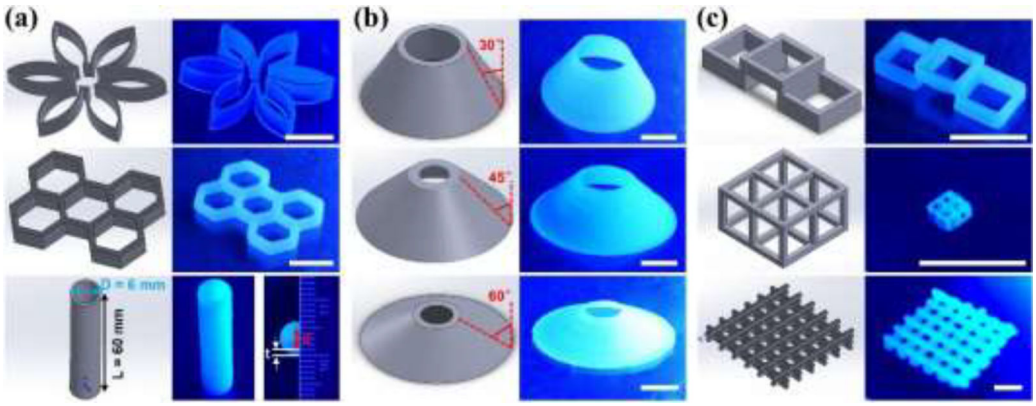

Figure 5.
CAD models and photographs of (a) stacked, (b) tiled, and (c) overhanging 3D printed structures. Scale bar: 1 cm.

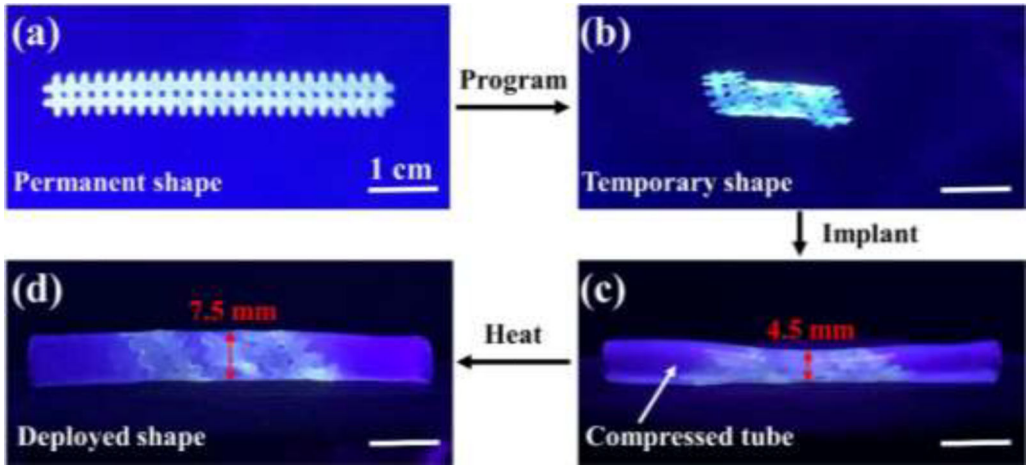

Figure 6.

In vitro testing of a printed vascular stent. (a) A permanent shape and (b) a temporary shape of a printed stent. The stent was printed from PGDA, then photo-crosslinked and thermally cured for 6 hours. (c) Implantation of the stent into a compressed silicone tube mimicking a narrowed blood vessel. (d) Enlarged tube diameter due to the deployment of the stent.

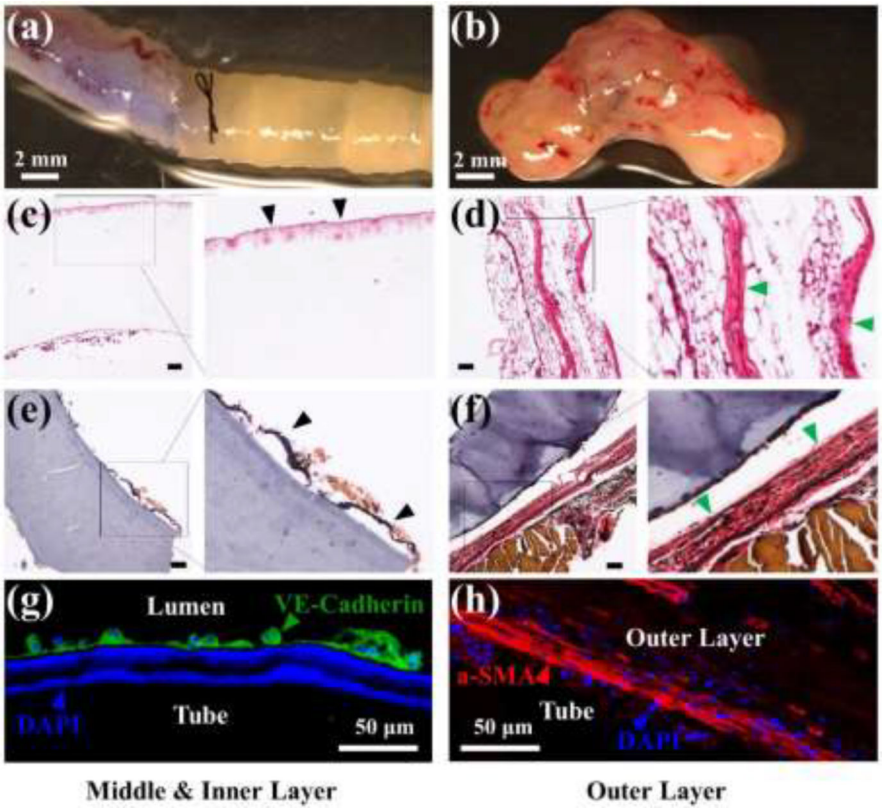

Figure 7.

In vivo remodeling of a vascular graft made of a c-PGDA tube which was thermally cured for 6 hours. Macroscopic images of the printed tube immediately after (a) and 14 days after (b) being anastomosed to a mouse aorta. H&E staining of the middle/inner (c) or outer layers (d) of a newly formed tissue after 14 days post-transplantation. Black arrows indicate the migration of cells into out layers and green arrows indicate potential adventitia growth. EVG staining of the middle/inner (e) or outer layers (f) of neo-tissue 14 days after tube grafting. Black arrows indicate inner elastin layer and green arrows indicate outer elastin layer. Scale bars for (c)-(f): 100 μm. (g) Image showing endothelial cells stained with VE-cadherin antibody (green). (h) Immunostaining of myofibroblast marker α-SMA (red, arrow). For (g) and (h), cell nuclei were stained with DAPI (blue).